On-Board Orbit Determination for a Deep Space CubeSat

By Boris SEGRET,[1] Daniel HESTROFFER,[2] Gary QUINSAC,[3] Marco AGNAN,[4] Jordan VANNITSEN,[4,5]

[1] Laboratory of Excellence for Exploration of Space Environments (LabEx ESEP), Paris Observatory, Paris, France

[2] Institut de Mecanique Celeste et de Calcul des Ephemerides (IMCCE), Paris Observatory, Paris, France

[3] Paris Sciences Lettres (PSL) Research University, Paris Observatory, Paris, France

[4] ODYSSEUS Space Co. Ltd., Tainan, Taiwan

[5] Department of Aeronautics and Aerospace (DAA), National Cheng Kung University (NCKU), Tainan, Taiwan

The low cost of CubeSats seems promising for deep space, swarms and constellations, provided that the operations remain at low cost too. A realistic autonomous Guidance, Navigation and Control (GNC) would contribute. Here we present our development road-map for an autonomous GNC technology and our progress with its on-board orbit determination (OD). The approach combines a continuous triangulation of foreground objects and a Kalman filter. The performance was assessed in a cruise context, for an interplanetary journey from Earth to Mars. Optical measurements of the directions of planets are assumed. A second case study was defined for a proximity context where a CubeSat accompanies a mothercraft in a rendez-vous mission to a double asteroid, flying at close range multiple times. The measurements are the directions of the asteroid, its neighbor moonlet, the Sun and possibly the mothercraft or distant planets. Monte-Carlo simulations were performed to propagate optical errors. The results show accuracies better than 100 kilometers in cruise at 1σ with conservative assumptions and still some possible improvements. The adaptations to the proximity context are also presented. This promising autonomous GNC could allow deep-space missions for a fraction of the cost of announced interplanetary CubeSats.

1. Introduction

A solution for autonomous orbit determination (OD) in deep space, either in interplanetary cruise or in exploring the vicinity of an asteroid, is investigated. The OD function is part of a full Guidance, Navigation and Control (GNC) technology called "BIRDY-T" that targets nano- and micro-satellites. The interest is to limit costly ground operations and unlock new scientific and commercial opportunities. The idea is to combine an asynchronous triangulation method, which cannot be accurate enough, with a Kalman filter. The on-board algorithm was prototyped and various optimization options were identified to improve the performance further.

Emerging nano-satellites with micro-propulsion offer new perspectives for constellations, formation flying swarms or even deep-space missions. But maneuvering each satellite individually from the ground could be expensive while the development of nano- and micro-satellites is expected at small cost, especially for CubeSats. Hence, the more autonomous the satellites, the lower the cost of operations. In the past, however, few deep space missions dealt with autonomous navigation, like NASA's Deep Space 1[4,5] or ESA's SMART-1.[6] The preferred approach is to compute its OD and its trajectory correction maneuvers (TCMs) from the ground. It is still true for small probes accompanying a mothercraft like PHILAE on ESA's ROSETTA.[7] A few past or proposed experiments rely on the heritage of missile guidance or consider landmark tracking, to reach, crash or land on a target (NASA's Deep Impact,[8] AIDA-DART,[12] landing of JAXA's HAYABUSA-1[14]) but not to navigate in its vicinity. When it comes to autonomous orbit determination, some early assessment (Folta et al, 2000[9]) states that a performance of 5 to 100 km for the accuracy in cruise is desirable as it could chal-
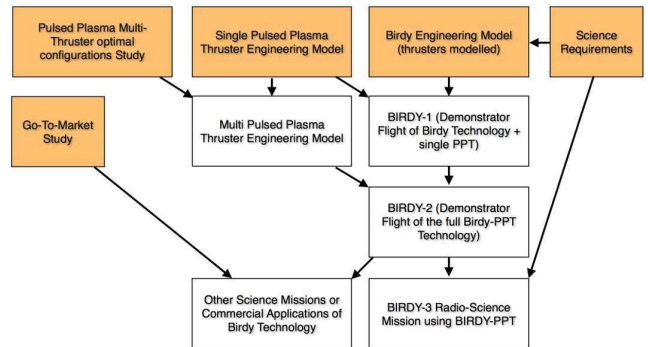

Fig. 1. BIRDY-T, a 5 to 6 year road-map.

lenge the standard approach of on-board propagators regularly re-calibrated from the ground.

In the next section, BIRDY-T technology road-map is briefly introduced. Mission profiles are presented, however they cannot be discussed in details as they are beyond the scope of this paper.

Then the on-board OD is presented with its associated ground segment. A triangulation method is defined for asynchronous measurements that produces a 3D-location (from a 26-unknown state vector). This location then feeds a Kalman filter. The assumptions on the CubeSat architecture and the optical accuracy σ_{in} are discussed. Monte-Carlo simulations are run to assess the resulting OD accuracy σ_{out} for multiple scenarios in cruise context (journey to Mars) and proximity context (to an asteroid).
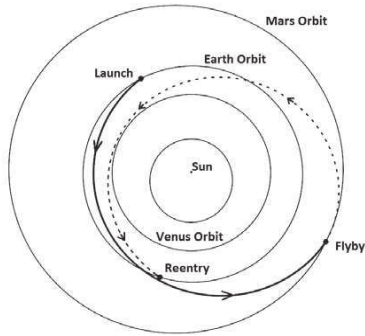
Fig. 2. Numerically Integrated Earth-Mars Free-Return trajectory (Solid Out, Dashed Return), Tito & al,[11] 2018-Jan-05 to 2019-May-21

Fig. 3. ESA's AIM proposal to Didymos.[13] Red arrows schematize multiple fly-bys of the CubeSat across the system (without sharp angles).

2. BIRDY-T, road-map for a GNC technology

The presented OD belongs to a wider technology development for an autonomous GNC technology called BIRDY-T, developed by a consortium of partners managed by Paris Observatory in France and National Cheng Kung University in Taiwan. A 5 to 6-year road-map organizing the main workpackages shwon in fig.1 was established. A first milestone is a versatile engineering bench "Birdy Engineering Model" with propulsion and autonomous GNC (including autonomous OD). Then two prototypes will fly in the vicinity of the Earth, before flying the first scientific deep-space mission for radio-science at an asteroid.

2.1. Propulsion and Orbit Control

The micro-propulsion assumed for BIRDY-T is a technology with Pulsed Plasma Thrusters (PPT) that has been developed by NCKU since 2011. Alternative solutions are also considered to assess whether they can fit the agility requirements, the power constraints and the ΔV budgets on small platforms. Moreover propulsion should likely be shared between multiple TCMs and attitude control needs with or without reaction wheels. The various options assume a ΔV-equivalent budget of a few tens to 100 m/s. On an indicative basis, perturbations in cruise, at NEO asteroid or at Mars are estimated at 10^{-7} to $10^{-9} N.m$ and micropulse torques at $10^{-6} N.m^{10)}$).

2.2. Multiple mission profiles

In addition of the micro-propulsion itself, orbit control strategies with continuous thrust are studied.

In cruise context there are two main strategies: shift corrections that bring the platform back on its initial trajectory, or new osculating orbits to reach the initial target (Mars for instance). Both strategies assume that the launcher (or cruise stage of the host mission where the CubeSat is in piggy-back) provides the initial interplanetary ΔV before jettisoning. The journey lasts several months and cruises over millions of kilometers. A limited number of TCMs will be run, more likely in the middle of the journey.

A journey from Earth to Mars in 2018 is considered (Fig. 2). The CubeSat is launched in piggy back of a host mission (study assumption) departing to Mars. After jettisoning and commissioning, the CubeSat is left in full autonomy to perform its own scientific mission as an autonomous probe, for instance for space weather monitoring, and its own TCM to reach Mars. W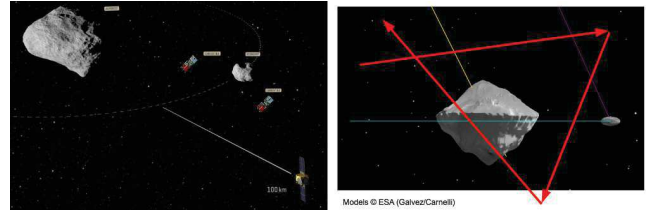hile approaching Mars, the scientific data are downloaded to the Earth via a data-relay with a Martian orbiter or lander. As a bonus, some situations reported by Tito[11] allow a flyby at Mars for a free-return trajectory to the Earth, which would double the scientific return.

In proximity operation context, typically in the vicinity of an asteroid, we consider either a quasi-elliptical orbit at very close range of the asteroid (few 100s to few 1000s meters) or hyperbolic arcs separated by large TCMs with a continuous thrust at larger distances (few km to tens of km) that we call "flyinglegs". Then the duration of an arc and a TCM is typically 1 to 2 days and the ground segment would update the navigation strategy only from time to time (once a week or every two weeks on AIM), keeping the tactics on board the CubeSat.

The CubeSat is released in situ by a mothercraft that stays in the vicinity of the explored asteroid and provides the data-relay. The CubeSat then flies multiple times across the system (Fig. 3) or in a self-maintained orbit. This context is inspired by ESA's AIDA-AIM mission for a rendez-vous at the double asteroid Didymos in 2022.[12,13] The Cubesat could go to risky locations over the main body or its moonlet and perform radio-science measurements. The goal is to probe the effect on the CubeSat itself of the local gravitational field. Then the mass density profile of the bodies can be reconstructed eventually. The radio-science data are produced with Earth-based and mothercraft-based ranging and Doppler, then relayed in S or X band by the mothercraft. Post-processed reconstructions concern the precise orbit of the CubeSat together with the gravitational models, using already well-mastered techniques. Here, the on-board orbit determination aims at increasing the autonomy of the CubeSat with a no-collision primary goal, then maximizing the scientific return and reducing the overall cost of operations.

Numerous issues related to these mission profiles are under study and will not be addressed here, namely: commissioning, TCM strategies, collision avoidance, radiation hardening, data-relay, beacon tracking from ground facilities (with VLBI), possible rescue uplink in cruise (with DSN), synchronized clocks, ultra-stable oscillator for radio-science.

3. On-board orbit determination

The developed OD intends to serve as inputs for all presented autonomous TCM while limiting ground operations at strategy level, in contrast to detailed TCM commands. As a result, the on-board orbit determination provides an estimated 3D-location of the CubeSat rather than the analytical parameters of an osculating orbit. In that respect this OD is strictly speaking a "3D-location determination".
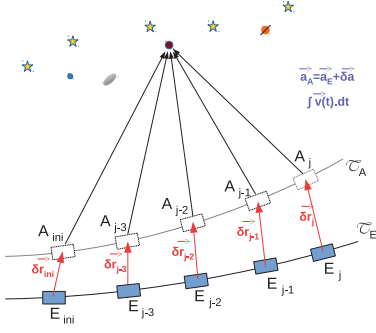
Fig. 4. Asynchronous triangulation: directions of bodies as seen from the actual Trajectory T_A are compared to the ones as seen from expected T_E.

Table 1. CRUISE context. Transverse errors for optical error σ_{in}=0.1" (with typical distances and angular diameters).

foreground bodies	typ.distance	ang.diam.	transv.error
Mars	1 AU	9"	73 km
Ceres	3 AU	0.5"	220 km
Jupiter	5 AU	40"	360 km
Saturn (& rings)	10 AU	15" (50")	730 km

Table 2. PROXIMITY context. Transverse errors for optical error σ_{in}=10" (with typical distances and angular diameters).

foreground bodies	typ.distance	ang.diam.	transv.error
Didymos (main)	30 km	1.5°	1.5 m
Didymos (moon)	30 km	0.3°	1.5 m
Mothercraft	100 km	10"	5 m

3.1. Overview of the algorithm

The estimate of the location is computed at a given epoch, on the basis of available optical measurements, with a prediction for the short term until new measurements are gathered.

The on-board algorithm combines a complex triangulation using a linear problem solver and a Kalman filter. The geometry problem is made linear by assuming small angular shifts between expected and actual directions of foreground bodies. It cannot be a direct triangulation because of the motion of the CubeSat between the measurements, thus we consider an asynchronous triangulation that requires more than three lines of sights. The ground segment has to prepare the expected situation to be stored on board as a reference. The result of the triangulation is a noisy 3D-shift with regard to the stored reference. Then the process is iterated and each output 3D-shift is injected as a new observation in a Kalman filter. After a number of iterations, the last Kalman-filtered prediction, its quality and a short term propagator are available.

3.2. Asynchronous triangulation

The basic triangulation requires in principle 3 directions of relatively close bodies. However, the measurements are not performed from the same point in space because the CubeSat needs time to orient its camera to each foreground body. Obviously, there is not any exact solution because of motion uncertainty and optical errors. Hence, more than 3 measurements are needed to over-constrain the geometry problem with its motion assumption. From N=5 optical measurements we build a system of $p = 26$ unknowns (N successive 3D-positions, i.e. $3N$ coordinates, N distances to foreground bodies, a 6-value state vector for the CubeSat) and $m = 27$ equations (3 equations per observation, i.e. $3N$, and $3(N - 1)$ equations to link the successive positions).

Comparing the actual and expected directions of foreground bodies (Fig. 4), the geometry problem is linearized by assuming small differences between varying lines of sights. The elementary system of linear equations for one given foreground body "i" is:

$$
\begin{bmatrix} 1 & 0 & 0 & \cos\phi_i \cos\lambda_i \\ 1 & 0 & 0 & \cos\phi_i \sin\lambda_i \\ 1 & 0 & 0 & \sin\phi_i \end{bmatrix} \cdot \begin{pmatrix} \delta x \\ \delta y \\ \delta z \\ d\rho_i \end{pmatrix}
$$
$$
= \begin{bmatrix} \rho_i \cos\phi_i \sin\lambda_i & \rho_i \sin\phi_i \cos\lambda_i \\ -\rho_i \cos\phi_i \cos\lambda_i & \rho_i \sin\phi_i \sin\lambda_i \\ 0 & -\rho_i \cos\phi_i \end{bmatrix} \cdot \begin{pmatrix} d\lambda_i \\ d\phi_i \end{pmatrix} \quad (1)
$$

where $(\lambda_i, \phi_i, \rho_i)$ are the expected longitude, latitude and distance of the observed body as computed in mission preparation, $(d\lambda_i, d\phi_i)$ is the measured angular shift between its expected and actual directions, and $(\delta x, \delta y, \delta z)$, $d\rho_i$ are respectively the unknown actual 3D-shift of the CubeSat from its expected location and the unknown radial difference to the body that is associated with this shift. There is a complicated non-linear relation that links $(\delta x, \delta y, \delta z)$ and $d\rho_i$ so we prefer to consider 4 independent unknowns, at the cost of additional measurements to constrain the system.

An optical accuracy of 0.1" is considered: it seems achievable with a navigation camera and multiple cross-correlations (MCC) in full-frame images.[5] A direct insight into the likely accuracy of the triangulation is given by the distances of foreground bodies and the optical accuracy of the measurements. Table 1 shows that, in cruise context, errors of several tens to several hundreds kilometers are expected transversely to the line of sight to each body.

Of course in proximity context the triangulation accuracy is expected to be much better. However the foreground objects may be too dark or too close (non ponctual, thus with irregular terminator), making the prediction of the photometric center tricky. Hopefully we can still expect interesting results due to the small distances, as shown in Table 2.

An efficient sun sensor with a 0.05° accuracy measuring the Sun direction from 1 AU would generate a transverse optical error of 150 000 km. Then it could seem useless to rely on this measurement, but it can also avoid co-planar situations and stabilize the Kalman filter.

Limitations and optimizations

The asynchronous triangulation outputs a p-value vector (p=26) including the N most likely positions of the CubeSat at the N successive measurements (N=5). This is done with an inversion that consists in minimizing a dimensionless quantitative criterion χ^2 resulting from the m-linear equation system (m=27): a minimum is expected with the p-value vector that nullifies all p partial derivatives of χ^2, i.e. a new linear system expressed with a p-square matrix whose rank is, in most cases, p and so the solution is unique.

Sometimes, the considered directions of foreground bodies become co-planar (e.g. same single body tracked from the orbital plane of the CubeSat), the matrix becomes non-reversible and the method cannot be used. This explains the request of non-co-planar directions for the foreground bodies and the rec-

ommendation to use at least several different bodies.

The method requires the inverse of a p-square matrix which may be complicated on board a CubeSat (p=26). Alternatives exist to avoid the use of an embedded high-level language function. At a prototype level, however, the results were obtained with the use of the MATLAB/OCTAVE embedded "inverse" function and an algorithm by steepest descent was also designed to make sure that a solution could be independent from "MATLAB auto-coding" or from private license considerations. The CPU-cost, however, has still to be studied in a CubeSat architecture.

Other triangulation methods and m-equation systems can be considered, in particular regarding the motion assumption between the successive N positions. In our results, the middle position among N=5 was found empirically to be the best and is kept for the rest of the process. This solution is likely to be improved.

3.3. Ground segment: propagator, trajectory solver

The on-board OD is to find the drift of the CubeSat from its expected trajectory, as prepared by the mission preparation and stored on board the CubeSat. It must be produced in association with the expected directions of pre-selected foreground bodies.

There is some flexibility on the representativeness of the predicted trajectory itself. The only requirement is to keep into a flight domain where the OD can be run, i.e. the volume around the trajectory where small angular shifts allow to linearize the geometry problem. In contrast, directions and distances of the foreground bodies as seen from the predicted trajectory (even if poorly reliable) must be very accurate: uncertainties on the raw ephemerides would come in addition of the optical errors and may prevent from relying on poorly known celestial bodies (in the asteroid belt, for instance). In addition, for the presented results, the relative ephemerides had to be produced at 10^{-8} degree and 1-*meter* accuracies to avoid numerical degeneracies while interpolating the expected situation at any given epoch. It has still some physical sense but polynomial descriptions could likely be preferred.

In cruise context, the expected trajectory and its relative ephemerides are stored in the CubeSat before launch. Several sets can be prepared to keep flexible with a change in the launch date. After launch, unless any rescue uplink, the basic mission profile does not anticipate any update. The ground segment must also include a trajectory solver that helps to assess whether a host mission opportunity can be used by the CubeSat with its own ΔV budget for a given scientific goal.

The situation is different in proximity context. Firstly, the mothercraft remains in the vicinity and can provide the CubeSat with data-relay, although the communications are likely very limited due to the main mission priorities. Several flying-legs are prepared and sent in advance to make the CubeSat autonomous for several days or weeks. Again a low reliability of the trajectory prediction is sufficient as long as the flight domain remains valid and the flight path secured (no collision risk due to local gravitational or non-gravitational uncertainties). The accuracy of the relative ephemerides of the close bodies is still very sensitive and also challenging (photometric center predictions). Secondly, the targeted science case is to probe the very local gravitational field. Thus the successive flying-legs shall allow several iterations on the models and ulti-

mately on the expected trajectories to confirm the models. The better the predicted trajectories, the better the knowledge on the asteroid system. In this context, the ground operations must be able to update trajectories and ephemerides and, by the way, to re-calibrate the position of the CubeSat from time to time (using ground tracking with VLBI, for instance).

To summarize, the ground segment requires a trajectory propagator, an easy access to raw ephemerides, various quality analyzers to sample the trajectories and ephemerides to be stored, and an easy interface to the mothercraft's operation pipeline. Also the gravitational fields must be modeled in full details and validated with replays of the past flying-legs, with a quick re-activity during operations. In addition, an improvement for the short-term on-board propagator is under study and could use the modeled local gravity field, as already processed by the ground segment, to be stored on board.

For all these reasons, the mission preparation is a critical part of the autonomous OD. A tailor-made ground segment is thus developed with experts in deep space dynamics and in on-board software architecture.

3.4. Kalman filter

The Kalman filter was built on the basis of a 9-value state vector (position, velocity, acceleration), with usual notations found in the literature:

$$\widehat{x_k} = A.\widehat{x_{k-1}} + B.u_k + W_k$$

$$with\ A = \begin{bmatrix} I_3 & dt.I_3 & 0_3 \\ 0_3 & I_3 & dt.I_3 \\ 0_3 & 0_3 & I_3 \end{bmatrix} \quad (2)$$

A is a simple transition matrix expressed in blocks (rank 3 identity and null matrices are noted I_3 and 0_3), the commands u_k are considered null (free fall) and the W_k is the accumulated process noise during dt, with initial estimates for the accuracy of the accelerations.

The observation model consists in injecting the selected best position found in the triangulation (the 3rd among N=5) as a z_k observation with a v_k error set on the results of the sensitivity tests that propagate the optical error σ_{in} into the triangulation algorithm:

$$z_k = C.x_{k-1} + v_k \quad (3)$$

where

$$C = \begin{bmatrix} I_3 & 0_3 & 0_3 \end{bmatrix}, z_k = \begin{pmatrix} x \\ y \\ z \end{pmatrix}_{from\ triangulation} \quad (4)$$

With this approach, the last a posteriori prediction provides an estimate of the state vector at the time of the 3rd measurement of the last triangulation, i.e. with a delay of two measurements. An additional a priori prediction can then be performed to estimate the location at the 5th measurement, i.e. at the current time. For the short term, additional a priori predictions can be obtained until a new set of measurements is available to perform a new triangulation, hence a new "observation", in Kalman filter terms.

One can note that this Kalman filter is far from being optimized and the results showed are likely to be improved. In particular, a first interesting option is to model the local gravitational field that is estimated by the propagator in the transition
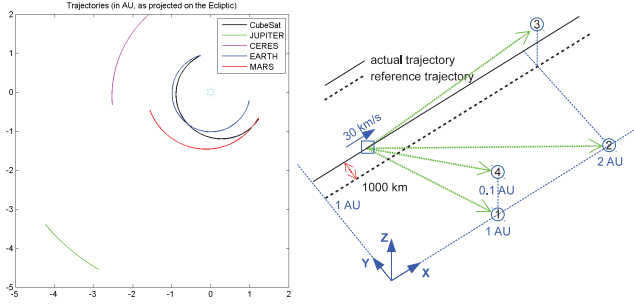
Fig. 5. CRUISE. Realistic Earth-Mars journey E2M (left, black) and fictional geometry Yline (right, black). In E2M the CubeSat and the foreground bodies move. In Yline, the CubeSat moves at constant velocity of 30 km/s and foreground objects (circled) are fixed.
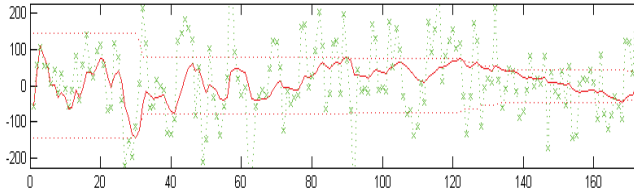

Fig. 6. Kalman filter behavior (example): OD transverse residual in km with a Kalman filter (red) and without (green) in function of the iterations.

matrix A and in the process noise W_k. A second option is to fine-tune the 3x3 co-variance matrix associated with v_k, using the predictable accuracy of the triangulation: indeed it can be intuitively expected as an ellipsoidal error oriented toward the line of sight of each foreground body rather than spherical as simulated yet.

4. Monte-Carlo simulations

4.1. Extent of the simulations

The presented results concern the cruise context. The scenario of a journey from Earth to Mars labeled E2M was simulated and, in addition, a fictional geometry labeled Yline — without any physical meaning — was also simulated to help interpreting the results. Both scenarios last ≈ 200 simulated days at a cruise velocity of ≈ 30 km/s. Foreground objects are distant from ≈ 1 to 5 AU, with 4 moving objects in E2M and 4 fixed objects in Yline (Fig. 5).

A scenario consists in setting up the trajectories (expected and actual), the conditions of the measurements (optical accuracy, frequency and sequence of observed bodies), and the number of iterations of the Kalman filter. Then, at regular intervals all over the scenario, a series of randomly noisy measurements is generated, the orbit determinations are processed as Monte-Carlo simulations to extract both standard deviations of the raw triangulation and of the Kalman filtering, in order to assess the added-value of each.

The Kalman filter behavior was monitored to get a clear view of its stabilization. Figure 6 provides an example showing the evolution of the OD residual transversely to the trajectory (a null residual means the OD provides the exact value of the shift between the expected and actual trajectories). A number of 192 iterations, at one per hour, was simulated in cruise context to represent 8 days of flight.

The number of Monte-Carlo simulations was checked to en-

Table 3. Summary of the simulated scenarios in cruise context, for each geometry (E2M or Yline) and each simulated σ_{in}

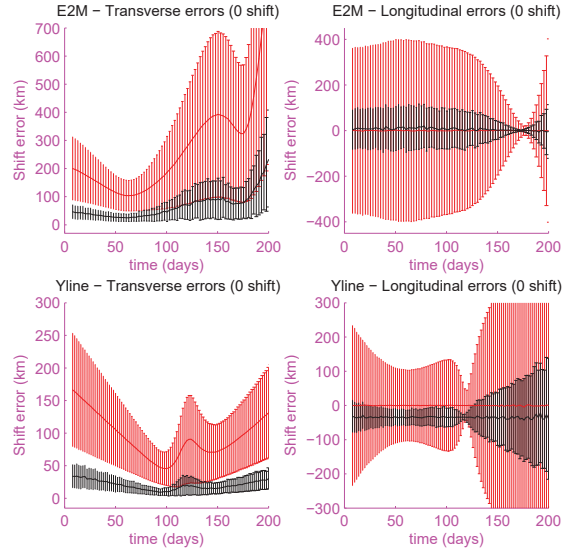| σ_{in}	E2M	Yline
0.2"	0 shift	0 shift
	0 shift	0 shift
0.1"	+X,+Z 1m/s ΔV	+X,+Y,+Z
	retrograde 1m/s ΔV	1000 km shifts
0.02"	0 shift	0 shift

Fig. 7. OD residuals in km: transverse (left), longitudinal (right) for E2M (top) and Yline (bottom) with "0 shift" scenarios over 200 simulated days. Error bars for triangulation alone (red) and after Kalman filter (black).

sure the mean values and the standard deviations were stabilized within 10% of variations for any random extraction of a half of the results. A typical number of 400 simulations of the whole OD process was found necessary for each interval of the scenario. For E2M the simulated actual trajectory is the propagation of the trajectory with initial conditions affected by a +1m/s ΔV compared to the expected. For Yline, the actual trajectory is simply shifted from the expected. Also, OD results were examined with "0 shift", i.e. the expected and actual trajectories are the same, and σ_{in} variations. For indicative information, these simulations took about 12 CPU-hours per scenario. Table 3 shows a summary of the 12 scenarios considered here for cruise context.

A detailed error budget of the OD is still mandatory but was not included yet. In particular, the effect of the drift of on-board clocks can play a sensitive role in the estimate of the expected location: then the expected ephemerides in cruise context (high velocities) and the expected local accelerations in proximity context (Kalman filter optimizations) can be affected.

4.2. OD performance in cruise context

With "0 shift" simulations, the intrinsic behavior of the OD can be assessed. Figure 7 shows that the error bars with the Kalman filter are lower than 100 km in the first 150 days of the scenarios, transversely and longitudinally. At the end of the scenarios, no possible drifts from the expected trajectories could explain the divergence (0 shift) so the increasing distance from foreground bodies must be suspected (Ceres and Jupiter in E2M, all bodies in Yline where the body #3 is reached at the $\approx 120^{th}$ day).
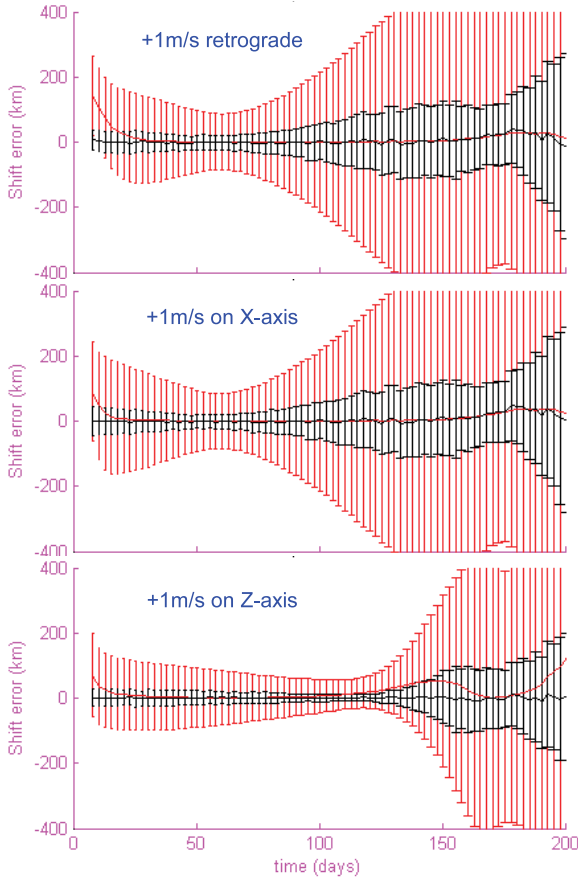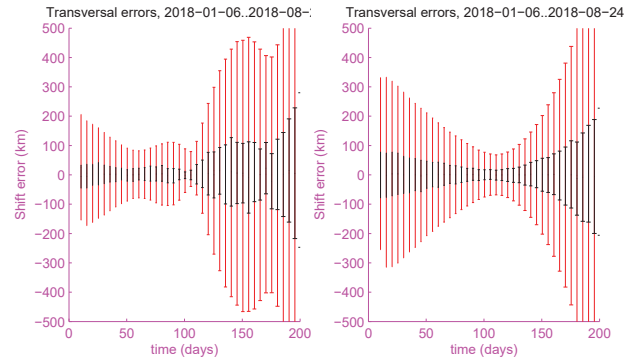
Fig. 9. OD transverse residuals in *km* for E2M with two sequences of foreground bodies: Earth-Ceres-Mars-Jupiter-Earth (left) and Jupiter-Ceres-Earth-Mars-Jupiter (right).

4.3. Primary factor: optical accuracy

It is not surprising that the primary factor is the optical accuracy σ_{in}. However the possible drift of on-board clocks was not studied in the OD performance yet.

Morover the OD process (triangulation and Kalman filter) produces σ_{out} values proportional to σ_{in} from 0.02" to 0.2". This was seen for E2M and Yline scenarios. This proportionality law makes the assessment for the optical accuracy easy: if only 1" accuracy is available, the 0 shift results would yield $3\sigma_{out} > 1000km$ which is rapidly far from acceptable.

4.4. Secondary factor: sequence of foreground bodies

Figure 9 shows that the shape of the uncertainties dramatically changes with the sequence of foreground bodies. Also the OD performance is very different, starting from $\sigma_{out} = 250km$ or $\sigma_{out} = 400km$ in the given examples. The same variability is seen with Yline scenarios. This result was obtained by running additional scenarios for E2M and Yline and only the best sequences were kept for further simulations. It also shows that a potentially important margin exists to improve the results with an improved strategy in the selection of foreground bodies to be measured.

4.5. Non-driver: intervals for optical measurements

The interval between successive optical measurements does not sensitively impact σ_{out}, which is a counter-intuitive result. Intervals from 12 *min* (5 measurements and 1 Kalman filter iteration per hour) to 6 *hr* (measurements and Kalman iteration every 30 *hr*) were tested and did not show significant changes in shapes and amplitudes. Hence, there is no specific requirement to put on this interval that remains flexible for attitude control considerations and overall duration of the OD after a number of Kalman filter iterations.

5. Adaptations to proximity context

An equivalent study has still to be done for the context of operations in the vicinity of an asteroid, with some important adaptations of the study in cruise context. At the time of issuing this paper, the scenarios are being generated and results are not yet available. A major analysis will be to compare the behaviors of flying-legs at distances of 5 to 50 *km* with controlled quasi-elliptical orbits much closer (below 1 *km* typically).

With flying-legs, the electric propulsion makes the TCM very smooth and a strategy that could naturally neutralize any possible unexpected drift of the CubeSat will be valuable. Thus,
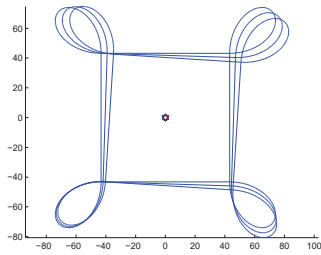

Fig. 8. OD transverse residuals in *km* for E2M scenarios where actual trajectories are propagated with initial conditions changed by +1m/s retrograde (top), on X-axis (middle), on Ecliptic Z-axis (bottom). Error bars for triangulation alone in red and after Kalman filter in black.

Mean values are usually not centered on zero, expressing that a bias is created by the OD. Some specific geometry in the scenario can explain that a bias is created. Sometimes, however, the bias is lower despite an increasing drift in the scenario than with these 0 shift scenarios. Thus further investigation is required.

In any case, the error bars without and with Kalman filter show a very positive effect of the Kalman filter: the bias and the standard deviation are significantly reduced. With Kalman filter σ_{out} is lower than 100 *km* that is the target objective, but the OD is only accurate at $3\sigma_{out}$ because of the bias.

Realistic results are shown in Fig. 8. In these scenarios, $1m/s$ was added to the velocity of the initial conditions of the expected trajectory and propagated to produce the actual simulation. The direct outputs of the triangulation suffer from some bias at the beginning of the scenarios (and also at the end but the shift may have gone out of the flight domain). Minima are not found at the same moments of the trajectory, which expresses the strong dependence to the specific geometry of the foreground bodies. Again the Kalman filter is very efficient at reducing the standard deviation as well as the possible bias.

With σ_{in}=0.1", if we assume that the simulation remains in the flight domain up to days ≈ 150, σ_{out} with Kalman filter is always below 100 *km* and most of the time below 50 *km*.

Fig. 10.   Schematic flying-legs with "TCM loops" in proximity context. The asteroid is at the center. 1 line + 1 loop is ≈ 80 *km* and lasts ≈ 2 days.

an idea is to consider TCM loops that theoretically finish at the point where they started, in order to assess the unknown perturbations in terms of a spherical, hopefully limited, error around the starting point of the TCM. This loop also allows direction changes in different planes. Simple mathematical formulas are being investigated like $\sin(kt).e^{it}$. Then multiple hyperbolic arcs like in Fig. 10 (with $k = 2$) can be planned in advance with a limited risk of fatal drift.

6.   Conclusion

We expect BIRDY-T to become a fully demonstrated autonomous deep space GNC for nano- and micro-satellites within 6 years, for a rough estimate of ≈ 5*M€*. This is in line, for comparison, with NASA's MarCO deep space mission that is scheduled to be launched to Mars in 2018 with a stated cost of ≈ *US* $ 15*M* for 2 CubeSats.

The on-board autonomous OD part of the GNC showed very promising results: the prototyped software yields an average 1-σ accuracy of ≈ 100 *km* in cruise context with on-board optical measurements at the 0.1"-accuracy level (as an initial requirement). The performance in a proximity context, to explore the vicinity of an asteroid, is about to be assessed. A tailor-made ground segment for mission preparations appears as a strategic component and special requirements in proximity operations were identified. However, a full error budget has still to be done, in particular with the drift of the on-board clock.

The presented approach still presents a large potential of improvements, so the already promising performances would be likely improved in the future. The primary improvements concern the model of motion during the optical measurements, with estimates of the local gravitational field, and an ellipsoidal model for the observation errors.

Acknowledgments

References

1) Segret, B. & al: *BIRDY: an interplanetary CubeSat to collect radiation data on the way to Mars and back to prepare the future manned missions*, SPIE Proceedings, Vol. 9150 (2014), Montreal, Quebec, doi: 10.1117/12.2056114.

2) Segret, B. & al.: *Orbit Determination for a deep-space CubeSat*, 6th Interplanetary CubeSat Workshop, Oxford, UK (2016).

3) Segret, B. & al.: *On-board Orbit Determination for a Deep-Space CubeSat*, 8th Summer School of the GRGS (Groupe de Recherche de Geodesie Spatiale, http://grgs.obs-mip.fr/), Aussois, France (2016).

4) Bhaskaran, S., Riedel, J.E., and Synnott, S.P.: *Autonomous optical navigation for interplanetary missions*, Jet Propulsion Laboratory, SPIE AA, Denver CO, 1996.

5) Riedel, J.E., and Bhaskaran, S.: *Using autonomous navigation for interplanetary missions: the validation of DEEP SPACE I Autonav* 4th IAA Low Cost Interplanetary Missions, Laurel (MA), IAA-L-1111, 2000.

6) Camino, O. & al.: *Smart-1 Operations Experience and Lessons Learnt*, 57th International Astronautical Congress Valencia, Spain, 2006, doi: 10.2514/6.IAC-06-B5.3.08.

7) Martin, T. & al.: *Flight Dynamics Analysis for Philae Landing Site Selection*, 25th International Symposium on Space Flight Dynamics, 2015.

8) Frauenholz, R.B & al.: *Deep Impact Navigation System Performance*, Journal of Spacecraft and Rockets, vol. 45, no. 1, pp. 3956, Jan. 2008, doi: 10.2514/1.24310.

9) Folta, D. C., Gramling, C. J., Long, A. C., Leung, D. S. P., and Belur, S. V.: *Autonomous navigation using celestial objects*, NASA Goddard Space Flight Center, AAS 99-439, 2000.

10) Quinsac, G. & al.: *Functional analysis of a CubeSat Attitude and Orbit Control System (AOCS) with propulsion for deepspace missions*, ESA-CNES 4S Symposium, Jun-2016.

11) Tito, Dennis A. & al.: *Feasibility Analysis for a Manned Mars Free-Return Mission in 2018*, Inspiration Mars, 2013.

12) Cheng, A. F., Galvez, A., Michel, P. & al.: *AIDA: Asteroid Impact & Deflection Assessment*, 64th International Astronautical Congress ©2013 IAF, vol. IAC-13-A3.4.8, 2013.

13) Galvez, A. & al.: *Asteroid Investigation Mission: the European contribution to the AIDA EU-US cooperation*, 24th International Symposium on Space Flight Dynamics, 2014.

14) Oshima, T., Kawaguchi, J. and Hagino, S.: *The Mission Operations of HAYABUSA Asteroid Explorer*, 57th International Astronautical Congress Valencia, Spain, 2006, AIAA doi:10.2514/6.IAC-06-C1.6.06.